PHYSICAL REVIEW D VOLUME 52, NUMBER 1 1 JULY 1995

# ARTICLES

## Search for neutral weakly interacting massive particles in the Fermilab Tevatron wideband neutrino beam

E. Gallas,* M. Abolins, R. Brock, W. G. Cobau,† R. W. Hatcher, D. P. Owen, G. J. Perkins, M. Tartaglia,‡ and H. Weerts
*Department of Physics and Astronomy, Michigan State University, East Lansing, Michigan 48824*

D. Bogert, S. Fuess, G. Koizumi, and L. Stutte
*Fermi National Accelerator Laboratory, Batavia, Illinois 60510*

J. I. Friedman, H. W. Kendall, V. Kistiakowsky, T. Lyons, L. S. Osborne, R. Pitt,§ L. Rosenson, U. Schneekloth,‖ B. Strongin,¶ and F. E. Taylor
*Massachusetts Institute of Technology Laboratory for Nuclear Science, Cambridge, Massachusetts 02139*

J. K. Walker, A. White,* and W. J. Womersley‡
*Department of Physics, University of Florida, Gainesville, Florida 32611*

(FMMF Collaboration)
(Received 29 December 1994)

A time-of-flight technique has been used to search for neutral weakly interacting massive particles in the wideband neutrino beam at the Fermilab Tevatron. Limits at the 90% confidence level are reported herein for (a) heavy neutrino production from the decay of heavy quark states, (b) massive objects directly produced in 800 GeV/$c$ $pN$ interactions that are noninteracting but unstable with a mean lifetime between $10^{-8}$ and $10^{-4}$ s, and (c) directly produced massive objects that are stable but weakly interacting with interaction cross sections between $10^{-29}$ and $10^{-31}$ cm$^2$.

PACS number(s): 14.80.−j, 13.15.+g, 14.60.St

### I. INTRODUCTION

The time-of-flight technique to search for neutral heavy particles in a beam dump was first suggested by Shrock [1]. With the use of scintillation counters operating parasitically within the FMMF neutrino detector, event times relative to the time of beam passage have been measured for neutrino events recorded during the 1987 Fermilab Tevatron fixed target run. The shape of the event time distribution depended on the inherent proton bunch shape and the time resolution of the apparatus. Events with measured event times outside the expected neutrino event time distributions were considered candidates for new particle production. The absence of such anomalous event times was used to set limits on new particle production in 800 GeV/$c$ proton-nucleon interactions based on an integrated number of live protons on target of $1.15 \times 10^{17}$. The method used in the present experiment is uniquely independent of the specific weakly interacting massive particle (WIMP) event topologies and therefore free from model-dependent background subtraction. A more detailed description of this analysis can be found elsewhere [2].

### II. EXPERIMENTAL SETUP

#### A. Neutrino beam time structure

Primary 800 GeV/$c$ protons struck the neutrino target (1 interaction length of BeO) in bunches which were synchronous with the accelerator rf clock, separated by 18.83 ns. The shape of each bunch in time was approximately Gaussian with a standard deviation of less than

*Present address: University of Texas at Arlington, Arlington, TX 76019.
†Present address: University of Maryland, College Park, MD 20742.
‡Present address: Fermi National Accelerator Laboratory, Batavia, IL 60510.
§Present address: AT&T, Naperville, IL, 60566.
‖Present address: DESY, Notkestrasse 85, 22603 Hamburg 52, Germany.
¶Present address: Varian Associates, Palo Alto, CA 94303.

 

1 ns [3]. The charged secondaries and their light decay neutrinos were highly relativistic, so they maintained the time structure of the proton beam as they traversed the focusing quadrupole triplet magnet train, the decay volume, and shielding before reaching the FMMF detector. The hadron and muon shield, located 542 m downstream of the neutrino target, consisted of an aluminum beam dump followed by a berm containing dirt with steel and lead inserts.

### B. Detector

A side view schematic of the FMMF detector is shown in Fig. 1. It was located 1599 m downstream of the neutrino target. The detector was designed for studying high-energy neutrino interactions. Details of the calorimeter and spectrometer are described elsewhere [4,5].

Briefly, the target/calorimeter consisted of alternating planes of target material (sand and steel shot) interleaved with flash chamber planes oriented in three views, and proportional tube planes in two views. The muon spectrometer measured the momentum and polarity of any high-energy muons that exited the downstream end of the calorimeter. Information from the flash chambers, proportional tube planes, and spectrometer was used to locate the event vertex, measure the event energy, find the position of the end of electromagnetic or hadronic showers, track muons and measure their momentum, and identify the final state event topology.

The aperture limiting the geometric acceptance of particles produced in the beam line was that of the active detector volume which subtended a half angle of approximately 1 mrad directly forward from the neutrino target.

Sixteen scintillation counters [the time-of-flight (TOF) counters] were arranged in four planes, as shown in Fig. 1, for the purpose of measuring event times relative to the rf clock. Each TOF counter consisted of a 200 cm $\times$31 cm $\times$2 cm slab of Bicron 408 scintillator viewed from each end by a 56AVP photomultiplier tube (PMT) through a Lucite$^{TM}$ light guide. Each TOF plane contained four TOF counters separated vertically by approximately 20 cm. The four TOF planes were located at 3.8, 6.3, 8.8, and 11.4 m downstream of the detector face. All planes were oriented in the same direction, with the length of the scintillator running in the horizontal direction perpendicular to the beam axis. The planes were staggered vertically to minimize gaps in coverage.

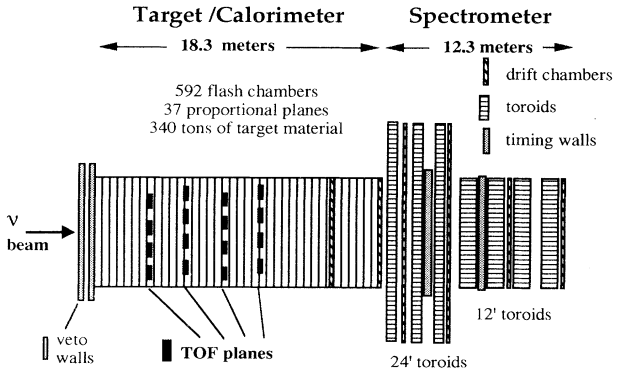


FIG. 1. Schematic of the FMMF neutrino detector.

The TOF counters had a simple geometry and coarse segmentation covering a large portion of the active calorimeter volume. Table I shows the longitudinal and transverse segmentation of the flash chambers, proportional tubes, and TOF counters for comparison.

Anode signals from each of the 32 PMT's were routed to discriminators set at both low and high thresholds. Both discriminator levels were typically satisfied for the traversal of a single minimum ionizing particle. Threshold crossing times relative to the rf clock signal from the accelerator were digitized and stored for each counter. PMT anode signals were also pulse-height analyzed and digitized.

## III. DATA ANALYSIS

Neutrinos interact with nucleons through the exchange of charged ($W^{\pm}$) or neutral ($Z$) gauge bosons, commonly referred to as *charged current* or *neutral current* interactions, respectively. Both event types result in hadronic showers with a broad range of energies; charged current events also have a high-energy muon in the final state, while neutral current events have a neutrino which escapes detection.

An event was designated CC (charged current candidate) if a high-energy muon was identified in the final state. The identified muon was required to have a track that emerged from the primary vertex with a length of at least 500 cm within the calorimeter if it exited the side of the calorimeter, or at least 1000 cm if it did not. The absence of such a topology qualified the event as NC (neutral current candidate).

The depth of the fiducial volume extended from the front face of the calorimeter to the position of the last TOF plane. Its cross section perpendicular to the beam direction was roughly circular with an equivalent area of 7.5 m$^2$. This fiducial volume had a cross-sectional area larger than that subtended by the TOF scintillator, but was far enough from the detector edge to ensure reasonable pattern recognition abilities. A neutrino event was classified as being in the fiducial volume if the event vertex was located within this volume. The fiducial mass was 98 metric tons.

Two triggers were used. The first trigger was satisfied if more than 5 GeV of energy was measured by the proportional tubes. The second trigger was designed to increase acceptance for CC events with very little hadronic shower energy; it required a small amount of energy in the calorimeter and a muon in the spectrometer. The combined trigger efficiency was found to be over 90% for total deposited energies of 5 GeV, rising to over 99% for energies above 10 GeV.

If signals from two TOF PMT's on the same side of the detector crossed the low threshold within 50 ns, then

TABLE I. Calorimeter segmentation parameters. The radiation and absorption length per plane express the number of radiation or absorption lengths between each unit of longitudinal segmentation for each detector subsystem.

| Calorimeter component | Flash chambers | Proportional tubes | TOF planes |
|---|---|---|---|
| Number of planes | 592 | 37 | 4 |
| Transverse segmentation | 5.77 mm | 10 cm | 30 cm (vertical) |
| Longitudinal segmentation | 3.2 cm | 46 cm | 2.0 m |
| Radiation length per plane | 0.22 | 3.6 | 17.85 |
| Absorption length per plane | 0.036 | 0.59 | 2.94 |

the TOF trigger condition was satisfied. Information from the time-of-flight counters was available much earlier than from the proportional tubes, which required 50 to 100 ns to make a triggering decision. Therefore, the TOF system was designed to trigger itself, digitize, and store all TOF signals, and then wait for a trigger signal from the detector.

The event sample consisted of all neutrino events with event vertices within the fiducial volume. The total 125 629 events were classified as shown in Table II.

## IV. NEUTRINO EVENT TIME DISTRIBUTIONS

A number of calculated corrections related to the threshold crossing times and PMT pulse heights were required before final event times could be computed. Using counters hit by single tracks these quantities were calculated in the off-line analysis as indicated below.

(1) The drift of the rf clock signal was monitored using event timing of muons in a calibration beam. Calibration beam interactions, recorded simultaneously with data taking, had the same time structure as the neutrino beam. Shifts in the rf clock signal were observed and correlated with changes in the outside temperature and changes in accelerator operations [6].

(2) Relative gains for the individual PMTs were determined. These pulse heights were the only available direct measurement of the total energy deposited in the scintillator.

(3) For each counter, the average time that the output pulse crossed the low level threshold was measured. All time measurements were corrected by these values, which set the average neutrino event time relative to a fixed phase of the rf clock to zero as well as accounted for channel specific cable length and electronics delays.

TABLE II. Shown here is the number of events, separated by CC and/or NC classification, in the fiducial volume, and/or timed using either the track or shower timing method. *Single counter* indicates measurements from a single counter were used to determine the event time, while *multiple counter* implies measurements from two or more counters were utilized.

| | CC events | NC events |
|---|---|---|
| In fiducial volume | 94 675 | 30 954 |
| Track timed (single counter) | 20 133 | – – – – – – |
| Track timed (multiple counter) | 12 485 | – – – – – – |
| Shower timed (multiple counter) | 11 385 | 12 139 |

After applying the above corrections, threshold crossing times were averaged to form an average PMT time $T_P$ for each PMT. An average counter time $T_C$ is formed by averaging the relevant $T_P$'s after correcting these measurements for the time required for the light to travel from the point of energy deposition to the photocathode. Since the pattern of energy deposition in the scintillator from muon tracks in CC events was different from that of hadronic showers in NC events, the timing analysis of each of these event topologies was treated separately as described in the following two subsections.

### A. Event timing using single muons

For the determination of the event time of CC events, only those TOF counters which were traversed by a muon were used. Transit-time corrections were well determined because of the precise spatial position of tracks provided by the flash chambers. All $T_C$ were folded into a single period of the rf clock extending from about $-9.5$ to 9.5 ns (a single period of the rf clock spans 18.83 ns). This shift, equal to an integral number of rf clock periods, was unambiguous for counters hit by an isolated track.

Pulse-height slewing of the timing signals was observed, producing systematically earlier time measurements when higher energy was deposited in the scintillator. $T_P$ measurements were therefore corrected in proportion to the pulse height. These corrections were as high as 2.5 ns. A nearly identical correlation in time shift versus pulse height was found in muon calibration event timing measurements. Before the $T_C$'s were averaged to obtain an event time $T_E^{\rm trk}$ (the event time determined using tracking), a number of cuts were imposed on $T_P$ and $T_C$ measurements to ensure that they were consistent with a signal produced from the traversal of single tracks [2].

In order to study any unanticipated systematics of the timing analysis, all events with $|T_C| \geq 3$ ns (160 in total) were scanned by eye. Figure 2 shows a typical CC event picture. From the detailed pattern of flash chamber hits, one can unambiguously distinguish a neutrino interaction from a cosmic ray or beam muon, as well as discern which counters were hit by muon tracks. A number of

anomalous events were identified. In particular, we note the following.

(1) Six events were due to cosmic ray interactions. Such events were found to have a flat $T_E^{\rm trk}$ distribution. Based on six cosmic ray events found with $|T_E^{\rm trk}| > 3$ ns, it is concluded that the total CC sample was contaminated with cosmic rays at less than a 0.03% level which has a negligible effect on the timing efficiency.

(2) In one event, corrections to a $T_C$ measurement were inappropriate because the pattern recognition algorithm was confused by flash chamber cells which fired as a result of residual ionization from a previous event.

(3) In 13 events, $T_C$ measurements were eliminated when either no muon was visible traversing that counter or the muon track ranged out before hitting the counter. These events were not eliminated from the event sample; rather $T_E^{\rm trk}$ was recalculated omitting those measurements deemed to be incorrect.

The timing resolution was better for events where two or more $T_C$'s were averaged to obtain $T_E^{\rm trk}$. Therefore, the timed CC sample was broken up into two parts: the first part consisted of all events timed using a single $T_C$ measurement, the second contained events timed utilizing two or more counters. The corresponding $T_E^{\rm trk}$ distri-

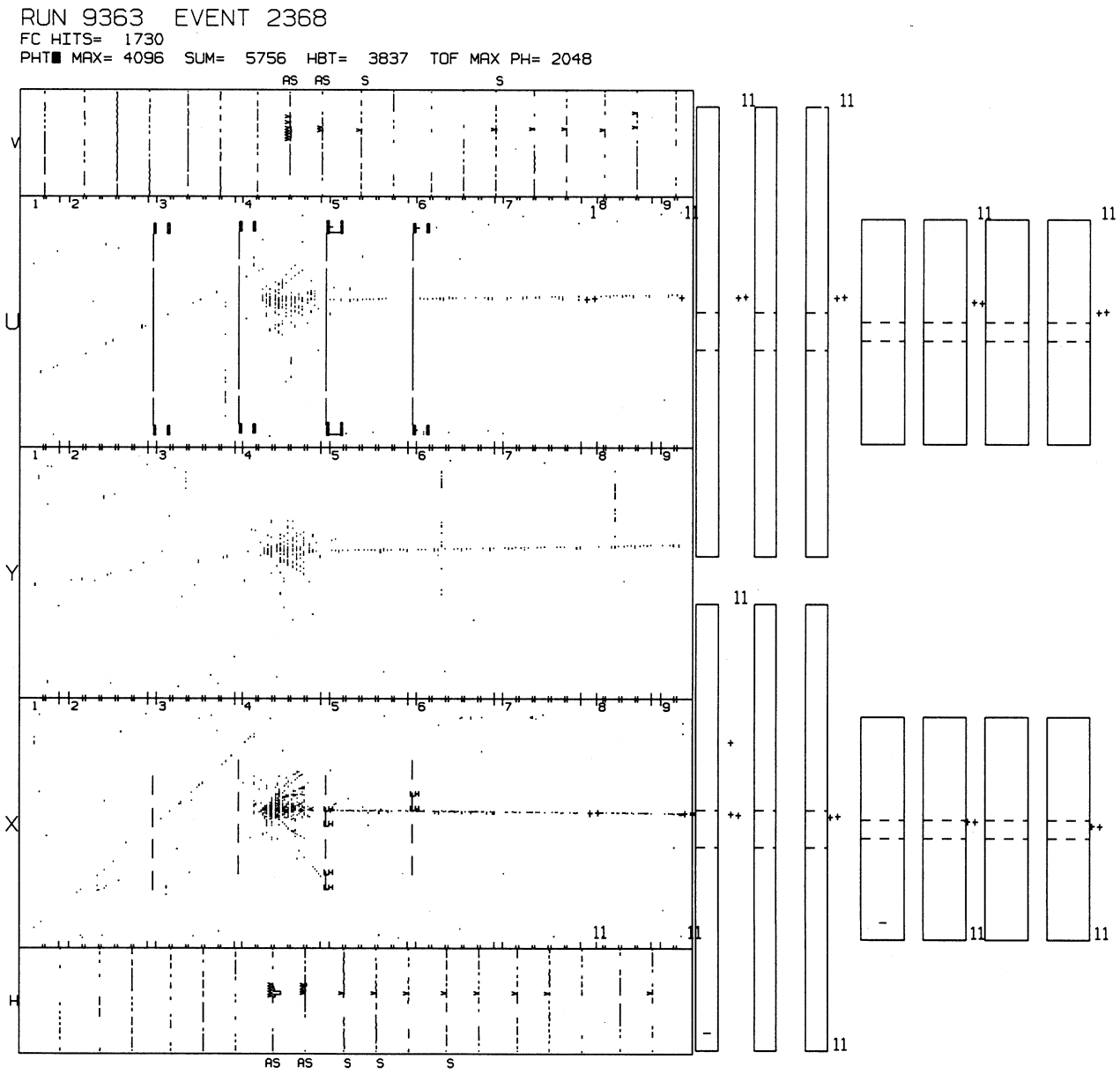


FIG. 2. A typical CC event in the FMMF detector.

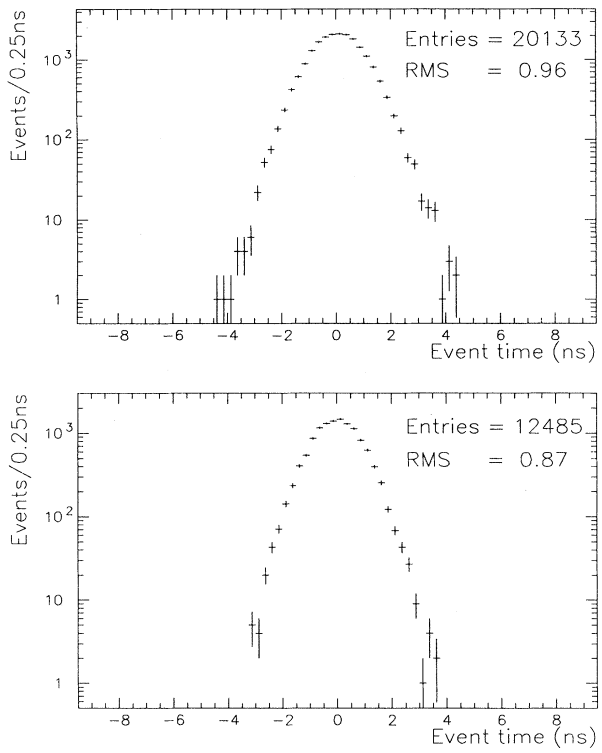


FIG. 3. The final CC event time distribution for (a) single counter timed events and (b) multiple counter timed events.

butions for the single and multiple counter timed events are shown in Figs. 3(a) and 3(b), respectively. In this representation smaller time measurements are the latest chronologically, while larger times are early.

The average timing efficiency was 34.5%. This efficiency was not independent of final state characteristics: The efficiency depended on the angle of the muon relative to the beam axis ($\theta_\mu$) as shown in Fig. 4. Also shown are the timing efficiencies for single and multiple counter

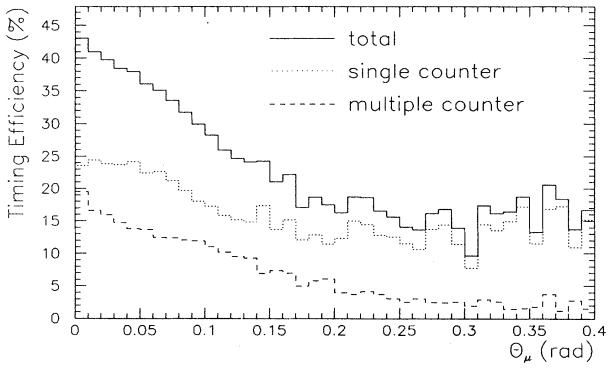


FIG. 4. The event timing efficiency as a function of the angle of the muon with the beam axis (solid line). The dotted and dashed lines indicate the timing efficiency for single and multiple counter timed CC events.

timed CC samples. These efficiencies were folded into Monte Carlo simulations of the acceptance.

In the single and multiple counter timed event samples, no events were observed in the time windows outside of $-4.5 < T_E^{\rm trk} < 4.5$ ns and $-3.25 < T_E^{\rm trk} < 3.75$ ns, respectively. These windows in which no events were observed, called the *TOF search windows,* along with the corresponding timing efficiency, were used to set limits on heavy neutrino and direct massive particle production as described below.

### B. Event timing using hadronic showers

Event times for NC events were determined using counters struck by the hadronic shower. The energy deposition of a shower in a TOF counter was not localized so time measurements were less precise and required more complicated corrections.

The timed CC sample, known to have $-4.5 < T_E^{\rm trk} < 4.5$ ns, was used to develop the algorithms for determining the event time for NC events because it was found empirically that timing characteristics of hadronic showers in NC and CC events were indistinguishable. The following corrections were applied.

For counters with both PMT pulse heights consistent with a minimum ionizing particle traversal, $T_C$'s were corrected just as in the track timing analysis.

When both pulse heights were greater, a number of measurables were found to be correlated with the apparent width of a shower intersecting a TOF counter. A shower width, determined using flash chamber information, was used to correct the measured times. In addition, consistently earlier time measurements were found in counters with a small vertical distance from the vertex to the center of the TOF counter utilized. It was presumed that this was due to neutrons, to which the TOF scintillator was sensitive, but the flash chambers were not. A correction proportional to the number of flash chamber hits seen in the flash chamber cells just upstream of the TOF counter utilized was also added.

When one pulse height of a counter was above the minimum ionizing range, or both were above the minimum ionizing range and a measured width was not available, $T_P$'s were shifted by an average amount obtained from all counters which had these characteristics. Further correlations between $T_P$ and other measurables, such as the number of flash chamber hits, were not observed.

After these timing corrections were applied, a number of consistency requirements similar to those made in the CC event timing analysis were imposed. The event time $T_E^{\rm shw}$ for NC as well as for CC events was obtained by averaging all available corrected time measurements passing the consistency criteria in each event. Events with $|T_E^{\rm shw}| > 5$ ns were scanned. A total of 154 events was scanned, 82 of which were classified as NC, the remaining 72 were classified as CC. Twenty-two cosmic ray events were found, all classified as NC, and they were eliminated from the sample.

To improve the timing resolution, events were also required to have at least two counters which satisfied the

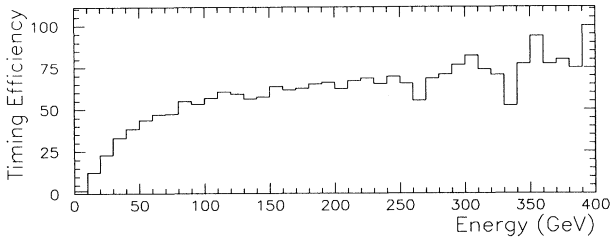


FIG. 5. The event timing efficiency as a function of shower energy in NC events.

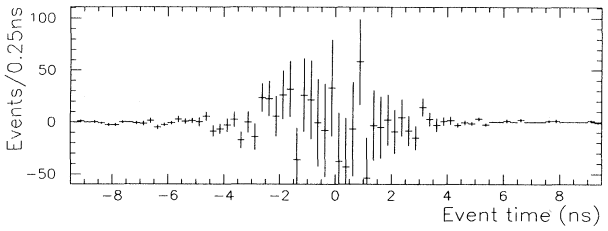


FIG. 7. Number of NC events above background as a function of time.

timing consistency criteria. For NC final states, the average multiple counter timing efficiency was 37%. This efficiency depended on the measured final state energy as shown in Fig. 5. The final $T_E^{\rm shw}$ distributions for NC and CC events are shown in Figs. 6(a) and 6(b), respectively. Because the timing characteristics of showers in CC and NC events were expected to be governed by the same systematics and since timed CC events were known to have $-4.5 < T_E^{\rm trk} < 4.5$ ns, the track timed CC event sample timed with the shower timing technique was presumed to form an estimate of the background due to neutrino induced NC events.

An event time window of $-5.0 < T_E^{\rm shw} < 5.0$ ns was chosen. The number of WIMP signal events corresponds to the number of NC events in excess of this background outside the event time window. The number of events in the CC distribution was normalized to the number of events in the NC distribution inside this event time window. The background subtracted NC distribution is shown in Fig. 7. The number of events outside the chosen time window was $-3.32 \pm 4.16$. For wider and narrower time windows, the number of events observed remained consistent with zero. The same is also true for the single counter timed NC events, though only the multiple counter timed NC event results were ultimately used to set limits on directly produced massive particles.

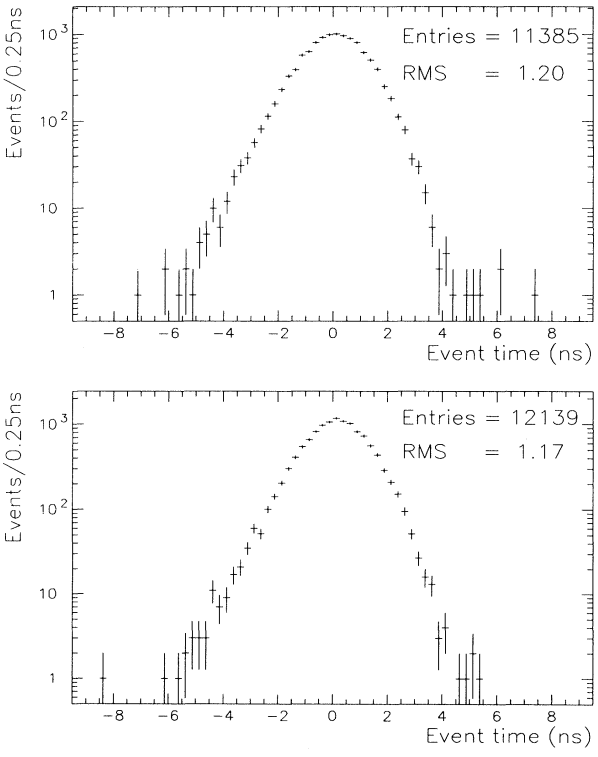


FIG. 6. The event time distribution obtained using the shower timing technique for (a) NC, and (b) CC events.

## V. LIMITS ON NEW PARTICLE PRODUCTION

A massive particle produced at the target or in the shielding will reach the detector later than a neutrino. The time delay, called the *time of flight,* is approximately given by

$$t = \frac{D}{2c}\left(\frac{M}{P}\right)^2, \qquad (1)$$

where $D$ is the distance traveled and $M$ and $P$ are the mass and momentum of the particle, respectively. This time of flight corresponds to the measured event time relative to the mean arrival time of the neutrino bunches in the detector, modulo 18.83 ns (one cycle of the accelerator rf clock). The signature of new massive particle in this detector was an event which occurs outside the expected time structure of the neutrino beam.

### A. Direct production limits

The possibility that a WIMP might be produced directly in 800 GeV/$c$ $pN$ interactions, and then interact or decay within the FMMF detector has been considered. Production in the center of mass was assumed to be similar to that measured in heavy quark production, that is, proportional to $(1-|x_F|)^n \exp(-b\sqrt{p_T^2+M^2})$, where $x_F$ is the Feynman scaling variable and $n$ and $b$ are empirically determined constants. For WIMP masses ranging from 1 to 20 GeV/$c^2$, the detector acceptance varied by less than a factor of 10 as the constants $n$ and $b$ varied in the ranges $1 \le n \le 10$ and $0.5 \le b \le 5.0$, respectively. These ranges were chosen as representative of what might be expected in the direct production of massive particles. For the limit results presented below, it has been assumed

that $n = 5.0$ and $b = 3.45$ as in a simulation [7] of the direct production of supersymmetric particles in a similar mass range.

Acceptance for directly produced particles was dominated by the convolution of geometric and *time-of-flight acceptance* (the fraction of geometrically accepted particles entering the FMMF detector in the TOF search window). For production at the beam dump from 800 GeV/$c$ protons, geometric acceptance ranged from 1.4% to 3%. The time-of-flight acceptance requirement is essentially a mass-dependent high-energy cutoff. If a particle was too energetic, it would not fall out of time sufficiently to appear different from a neutrino event. Because of this cutoff, the apparatus was not sensitive to WIMPs with masses below about 0.5 GeV/$c^2$.

Overall acceptance (including geometric, time-of-flight, and trigger acceptance) for WIMPs directly produced at the beam dump ranged from $1.0 \times 10^{-4}$ to $2.2 \times 10^{-2}$ for masses of 1 to 20 GeV/$c^2$, respectively. Despite increased TOF acceptance for production at the primary target (target was 500 m upstream of the dump), overall acceptance for target production was typically about two times lower than for production at the beam dump due to decreased geometric acceptance.

For this general model, the independent parameters are the production cross section $\sigma$, the mass $M$, the branching ratio $B$ to produce the indicated final state, and either (a) the mean lifetime $\tau$ for noninteracting unstable particles which decay in the detector or (b) the interaction cross section $\sigma_{\rm int}$ for stable weakly interacting particles. A linear atomic weight dependence of the production cross section was assumed.

For the case of an unstable WIMP decaying to final states with muons, limits on particle mass versus $\log_{10}\tau$ are shown in Fig. 8, where contours of equal 90% C.L. upper limits on $\sigma B$ are indicated. The solid curves represent the FMMF results, while dashed curves represent results of NA3 [8], a short beam dump experiment performed at CERN designed to look for charged or neutral massive ($> 1$ GeV/$c^2$) particles with $10^{-11} < \tau < 10^{-8}$ s. The FMMF and NA3 experiments were complementary in sensitivities. The long beam line made FMMF insensitive to shorter lifetimes, but when combined with the higher integrated luminosity, FMMF was more sensitive to longer lifetimes despite lower acceptances.

The equivalent contours for final states with no muon (NC class) were similar but less exclusive by a factor of approximately 2 in $\sigma B$ as shown in Fig. 9. Again, the solid contours represent the FMMF results. The dashed curves show the comparable contours from the NA3 experiment for the specific final state $\pi^{\pm}\pi^{\mp} + X$ (inclusive). The NA3 result for a $\pi^{\pm}e^{\mp}$ final state (not shown) was similar but less exclusive.

Shown in Fig. 10 are contours of equal 90% C.L. upper limits for $\sigma B$ as a function of mass and interaction cross section for stable weakly interacting particles for (a) final states that contain a muon and (b) final states without a muon.

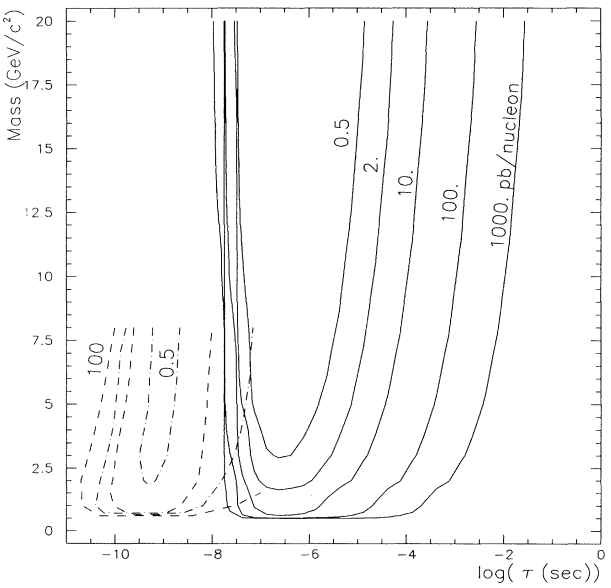


FIG. 8. For final states that contain a muon, contours of equal 90% C.L. upper limits on production cross section times branching ratio (pb/nucleon) are shown as a function of mass and lifetime for noninteracting unstable particles. Solid curves represent the FMMF results. Dashed curves indicate results from the NA3 experiment for identical $\sigma B$ and specific final state $\mu + \pi$ or $\mu + \mu$.

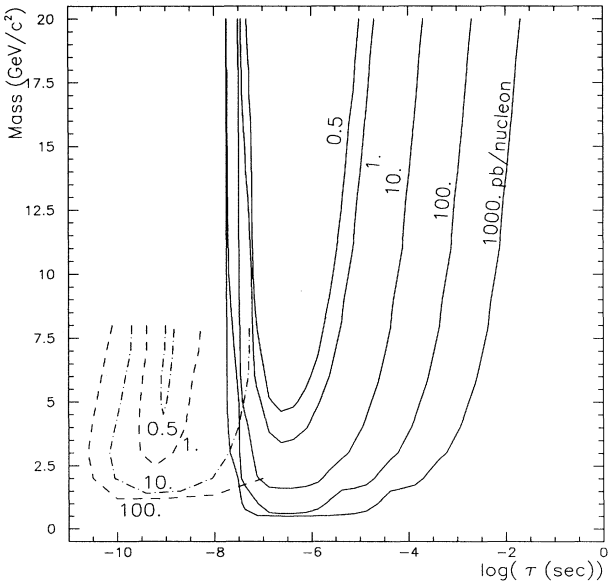


FIG. 9. For final states that do not contain a muon, contours of equal 90% C.L. upper limits on production cross section times branching ratio (pb/nucleon) are shown as a function of mass and lifetime for noninteracting unstable particles. Solid curves represent the FMMF results. Dashed curves indicate results from the NA3 experiment for identical $\sigma B$ and specific final state $\pi^{\pm}\pi^{\mp} + X$ (inclusive).

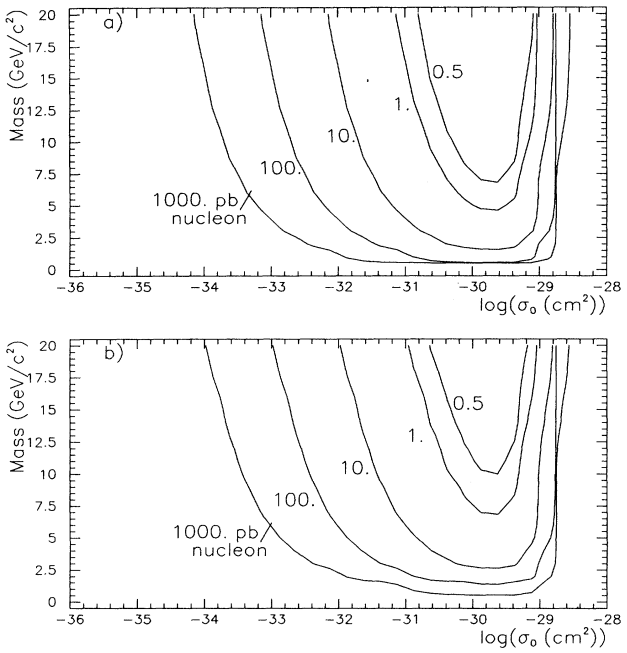


FIG. 10. Contours of equal 90% C.L. upper limits on production cross section times branching ratio (pb/nucleon) are shown as a function of mass and interaction cross section for stable weakly interacting particles for (a) final states that contain a muon, and (b) final states that do not contain a muon.

### B. A model for heavy neutrino production

An extension of the standard model [9] in which the $\mu$ flavor weak neutrino eigenstate is a superposition of the conventional light $\nu_\mu$ mass eigenstate and a new heavy eigenstate $\nu_H$ has been investigated. The new state couples to $\mu^\pm$ with strength $\propto |U_{\mu H}|^2$. These heavy eigenstates would manifest themselves in the leptonic decays of heavy quark states such as in the decays $D^\pm$ or $D_s^\pm \to \nu_H + \mu^\pm$, provided the kinematic threshold was satisfied. In this scenario, heavy quarks would be produced in the beam line and decay into a long-lived heavy neutrino which decays in the detector.

There were a number of sources of charmed mesons in the neutrino beam line including 800 GeV/$c$ protons interacting in the primary target and the beam dump, and secondary beam particles interacting in the beam dump such as $\pi^\pm$, $K^\pm$, and $p^\pm$. To simulate charm production, differential and total cross section results from a number of charm hadroproduction experiments were used [10–12]. The energy dependence of the charm production cross section in both $pN$ and $\pi N$ interactions was taken from Ref. [13].

A Monte Carlo simulation of the full production and decay chain was used to determine the number of expected events seen in the FMMF detector. In addition to the charm production parametrizations above, this simulation also included a theoretical model for expected lifetime and branching ratios for the production and decay of the heavy neutrino [9]. These predictions vary with heavy neutrino mass and mixing parameter, which were the two independent parameters for this model.

Geometric acceptance rose steadily with mass, ranging from 0.3% to 1.4% for masses from 0.5 to 1.8 GeV/$c^2$, respectively, for production at the beam dump. This acceptance was lower than that in the direct production case because of the $D$ decay kinematics. Acceptance improved for masses approaching the mass of the parent $D$ meson. The overall acceptance for heavy neutrinos ranged from $1 \times 10^{-5}$ to $7 \times 10^{-4}$ for masses of 0.5 to 1.8 GeV/$c^2$, respectively.

Figure 11 shows the results of the current experiment superimposed with the results of other experiments (listed in Ref. [14]) searching for massive neutrinos produced via similar mechanisms.[1]

Other beam dump experiments [14,15] have ruled out this phase space previously. However, it should be emphasized that the method used in the present experiment is completely different from those of the other experiments cited. The present experiment does not rely on specific decay topologies for the detection of such particles and no physics background subtraction is involved in this analysis. Results from the CERN $e^+e^-$ collider LEP have also ruled out such states, if it is assumed that the $Z$ boson coupling to heavy neutrinos is not suppressed.

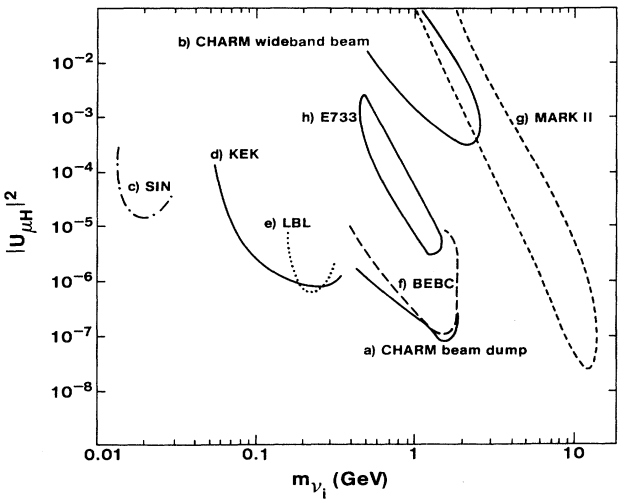


FIG. 11. Limits at the 90% confidence level on $|U_{\mu H}|^2$ as a function of the neutrino mass: (a) limits obtained in the CHARM beam dump experiment; (b) limits obtained in the CHARM wideband neutrino beam; (c) limits obtained studying the decay $\pi \to \nu\mu$ at SIN; (d) limits from the study of the decay $K \to \nu\mu$ at KEK; (e) limits from the study of the decay $K \to \nu\mu\nu^*$ at LBL; (f) limits obtained in the Big European Bubble Chamber (BEBC) beam dump; (g) limits obtained from the Mark II experiment; and (h) limits from FMMF (E733) experiment.

[1]The MARK II experiment searches for massive neutrinos in $e^+e^-$ interactions rather than from the decay of hadronic states.

## VI. CONCLUSION

At the 90% confidence level, limits have been set on massive objects directly produced in 800 GeV/$c$ $pN$ interactions that are noninteracting but unstable with mean lifetime between $10^{-8}$ and $10^{-4}$ s and directly produced massive objects that are stable but weakly interacting with interaction cross sections between $10^{-29}$ and $10^{-31}$ cm$^2$. Additionally, limits have been set on heavy neutrino production from the decay of heavy quark states.

## ACKNOWLEDGMENTS

This research was supported in part by the U.S. Department of Energy and the National Science Foundation. We wish to also acknowledge technical help from Bill Burley, Ron Olsen, Ron Richards, Sharon Joy, and the Fermilab staff.

[1] R. E. Shrock, Phys. Rev. Lett. **26**, 1688 (1978).
[2] E. J. Gallas, Ph.D. thesis, Michigan State University, 1993.
[3] Kurt Owen (private communication).
[4] W. J. Womersley *et al.*, Nucl. Instrum. Methods A **267**, 49 (1988).
[5] J. Bofill *et al.*, Phys. Rev. D **36**, 3309 (1987).
[6] M. A. Tartaglia, in *New Directions in Neutrino Physics at Fermilab*, Proceedings of the Workshop, Batavia, Illinois, 1988, edited by R. Bernstein (Fermilab, Batavia, 1988).
[7] A. M. Cooper-Sarkar *et al.*, Phys. Lett. **160B**, 212 (1983).
[8] J. Badier *et al.*, Z. Phys. C **31**, 21 (1986).
[9] M. Gronau, C. N. Leung, and J. L. Rosner, Phys. Rev. D **29**, 2539 (1984).
[10] R. Ammar *et al.*, Phys. Rev. Lett. **61**, 2185 (1988).
[11] M. Aguilar-Benitez *et al.*, Phys. Lett. **135**, 237 (1984).
[12] M. Aguilar-Benitez *et al.*, Z. Phys. C **31**, 491 (1986).
[13] R. K. Ellis and C. Quigg, FNAL Report No. FN-445, 1987 (unpublished).
[14] J. Dorenbosch *et al.*, Phys. Lett. **166B**, 473 (1986).
[15] A. M. Cooper-Sarkar *et al.*, Phys. Lett. **160B**, 207 (1985).